Vol. 14, pp. 49–55 (2017)
doi: 10.2142/biophysico.14.0_49

Biophysics and Physicobiology
https://www.jstage.jst.go.jp/browse/biophysico/

Regular Article

Existence of two O-like intermediates in the photocycle of *Acetabularia* rhodopsin II, a light-driven proton pump from a marine alga

Jun Tamogami[1], Takashi Kikukawa[2,3], Toshifumi Nara[1], Makoto Demura[2,3], Tomomi Kimura-Someya[4,5], Mikako Shirouzu[4,5], Shigeyuki Yokoyama[4,6], Seiji Miyauchi[1,7], Kazumi Shimono[1,7] and Naoki Kamo[1,2]

[1]*College of Pharmaceutical Sciences, Matsuyama University, Matsuyama, Ehime 790-8578, Japan*
[2]*Faculty of Advanced Life Science, Hokkaido University, Sapporo 060-0810, Japan*
[3]*Global Station for Soft Matter, Global Institution for Collaborative Research and Education, Hokkaido University, Sapporo 001-0021, Japan*
[4]*RIKEN Systems and Structural Biology Center, Yokohama 230-0045, Japan*
[5]*RIKEN Center for Life Science Technologies, Yokohama 230-0045, Japan*
[6]*RIKEN Structural Biology Laboratory, Yokohama 230-0045, Japan*
[7]*Graduate School of Pharmaceutical Sciences, Toho University, Funabashi, Chiba 274-8510, Japan*

Received December 6, 2016; accepted March 2, 2017

A spectrally silent change is often observed in the photocycle of microbial rhodopsins. Here, we suggest the presence of two O intermediates in the photocycle of *Acetabularia* rhodopsin II (ARII or also called Ace2), a light-driven algal proton pump from *Acetabularia acetabulum*. ARII exhibits a photocycle including a quasi-equilibrium state of M, N, and O (M⇄N⇄O→) at near neutral and above pH values. However, acidification of the medium below pH ~5.5 causes no accumulation of N, resulting in that the photocycle of ARII can be described as an irreversible scheme (M→O→). This may facilitate the investigation of the latter part of the photocycle, especially the rise and decay of O, during which molecular events have not been sufficiently understood. Thus we analyzed the photocycle under acidic conditions (pH ≤ 5.5). Analysis of the absorbance change at 610 nm, which mainly monitors the fractional concentration changes of K and O, was performed and revealed a photocycle scheme containing two sequential O-states with the different molar extinction coefficients. These photoproducts, termed O_1 and O_2, may be even produced at physiological pH, although they are not clearly observed under this condition due to the existence of a long M-N-O equilibrium.

Key words: retinal, isomerization, Schiff base switching, spectrally silent transition, microbial rhodopsin

Corresponding author: Jun Tamogami, Laboratory of Biophysical Chemistry, College of Pharmaceutical Sciences, Matsuyama University, 4-2 Bunkyo-cho, Matsuyama, Ehime 790-8578, Japan.
e-mail: jtamoga@cc.matsuyama-u.ac.jp

Microbial rhodopsins undergo a cyclic photochemical reaction (photocycle) induced by photoexcitation of all-*trans* retinal (RET) as a chromophore. The photolyzed protein

◀ **Significance** ▶

The latter half of the photocycle of microbial rhodopsins remains incompletely understood. Although the transition from N to O intermediate is accompanied by thermal reisomerization of retinal chromophore and accessibility switch of the protonated Schiff base, it has been an unsolved problem which event occurs first, even in bacteriorhodopsin (BR), the most intensively-studied microbial rhodopsin. The present work revealed the formation of two O-states in the latter part of the photocycle of *Acetabularia* rhodopsin II, a BR-like light-driven proton pump from a marine alga. This finding would help us to understand the latter molecular event in the photocycle of microbial rhodopsins.

after all-*trans* to 13-*cis* isomerization of RET thermally returns to the initial unphotolyzed state. During their respective photocycles, several spectroscopically different photoproducts, referred to as K, L, M, N, and O, appear in a sequential manner [1]. The transitions between successive states are accompanied by several chemical and structural events, such as reisomerization of RET, proton (or other ion species such as Cl^- and Na^+) movement, and conformational changes of the protein, playing a crucial role in exerting the respective functions of microbial rhodopsins [1]. Among four microbial rhodopsins in haloarchaea, the photocycles of bacteriorhodopsin (BR) as a light-driven proton pump and two sensory rhodopsins (SRI and SRII) commonly include a blue-shifted M with deprotonated retinal Schiff base (SB). However, the decay of M in BR is relatively fast, whereas those in SRI and SRII are slow due to a defect in efficient SB reprotonation. On the other hand, M is not found in the photocycle of halorhodopsin (HR), a light-driven inward chloride pump. Although the transitions between each photointermediate described above (K-O) occur with large spectral shift, transitions without apparent spectral changes are also often observed in their photocycles [2]. The most famous example of this is found in the first half of the photocycle of BR [3]. A spectrally silent transition between two M-like substates, M_1 and M_2, which works as the accessibility switching process for SB from the extracellular (EC) side to cytoplasmic (CP) side, leads to unidirectional outward proton transport by BR [3]. Another example is the L_1-L_2 transition that occurs in the photocycle of HR. In this transition, it has been deduced that the position of Cl^- changes inside the protein [1,4,5]. In addition, it is considered that the formation of multiple M species in SRI and SRII may participate in signal transduction to a transducer by F-helix tilting [6,7]. Therefore, spectrally unchanged processes during the photocycle may also happen on other intermediates and be worth further investigation if they exist.

In contrast with the first half of the photocycle, the second half of the photocycle has been incompletely understood. The presence of two N-states after M was reported in BR [3]. The N_1 (N) to N_2 (N′) conversion changes the connectivity of a proton donor to SB ($D96^{BR}$) from SB at the intracellular surface to take up a proton from the CP aqueous phase [3]. This process also serves for the regulation of the direction of proton translocation like the M_1-M_2 conversion. The N-O transition accompanies the isomerization. The isomerization-switch-transfer (IST) model by Haupts *et al.* assumes that the switch (orientation change of N-H of SBH^+ between CP and EC) occurs after the isomerization [8]. On the other hand, Wang *et al.* carried out the molecular dynamic (MD) simulations during the N-O transition of BR, and the first switch is followed by the isomerization in the latter part of the photocycle, which is contrast to IST model [9]. Wang *et al.* thought the important role of the interaction of SBH^+ with deprotonated $D212^{BR}$ in EC [9].

In this article, we report the presence of two O states in the photocycle of *Acetabularia* rhodopsin II (ARII or also called Ace2), which is one of two eukaryotic light-driven proton pump homologues from the marine alga *Acetabularia acetabulum* [10,11]. As reported previously, the latter half of the photocycle of ARII at neutral pH is described as $M \rightleftarrows N \rightleftarrows O \rightarrow ARII' \rightarrow ARII$ [11]. The existence of reversible reactions between M, N and O makes analysis of the photocycle complicated. However, the equilibrium between M and N in the above scheme shifts toward M due to a rapid back reaction at acidic pH (<~5.5). In addition, the N→O reaction is fast under this condition because the medium pH is below the pK_a (5.9 or 6.3) of $D92^{ARII}$ (corresponding to $D96^{BR}$) during H^+-uptake at N-decay [11]. Therefore, N is not accumulated at pH <~5.5, allowing the scheme to be simplified as $M \rightarrow O \rightarrow ARII' \rightarrow ARII$. Consequently, the kinetic analysis becomes easy, and we found two O intermediates in the photocycle of ARII.

Materials and Methods

Sample preparation

The procedure for the synthesis of ARII protein by cell-free expression and its purification method were the same as previously described [10,11]. ARII solubilized with 0.05% n-dodecyl-β-D-maltoside (DDM) was used.

Flash photolysis

Measurements were performed by using the same apparatus and procedure described previously [12]. Absorbance changes generated by the excitation of proteins with a laser pulse (Nd:YAG 532 nm, 7 ns, 5 mJ/pulse) were collected at three characteristic wavelengths (400, 520, and 610 nm) at 20°C. The experimental medium was a solution containing 400 mM NaCl and 6-mixed buffer (citrate, MES, HEPES, MOPS, CHES, CAPS, at 2 mM each). Data analysis was conducted using the Microcal Origin software (OriginLab, Microcal Software).

Results and Discussion

To detect three characteristic photocycle intermediates, K, M, and O, flash-induced absorbance changes were measured at three selected wavelengths at three different pH values, as shown in Figure 1. Note that L cannot be clearly observed, likely due to kinetics. The obtained ΔA_{400} and ΔA_{520} signals mainly reflect concentration changes of M and the original pigment (ARII), respectively. On the other hand, two red-shifted photointermediates, K- and O-states, have an absorbance maximum wavelength (λ_{max}) at a similar red-shifted spectral range [11]. It is worth noting that the absorbance change at 610 nm over the early time range prior to ~0.02 ms represents the time-dependent fractional concentration change of K, whereas the rise and decay of O are detected at the latter time range.

In agreement with the simplified scheme described above,

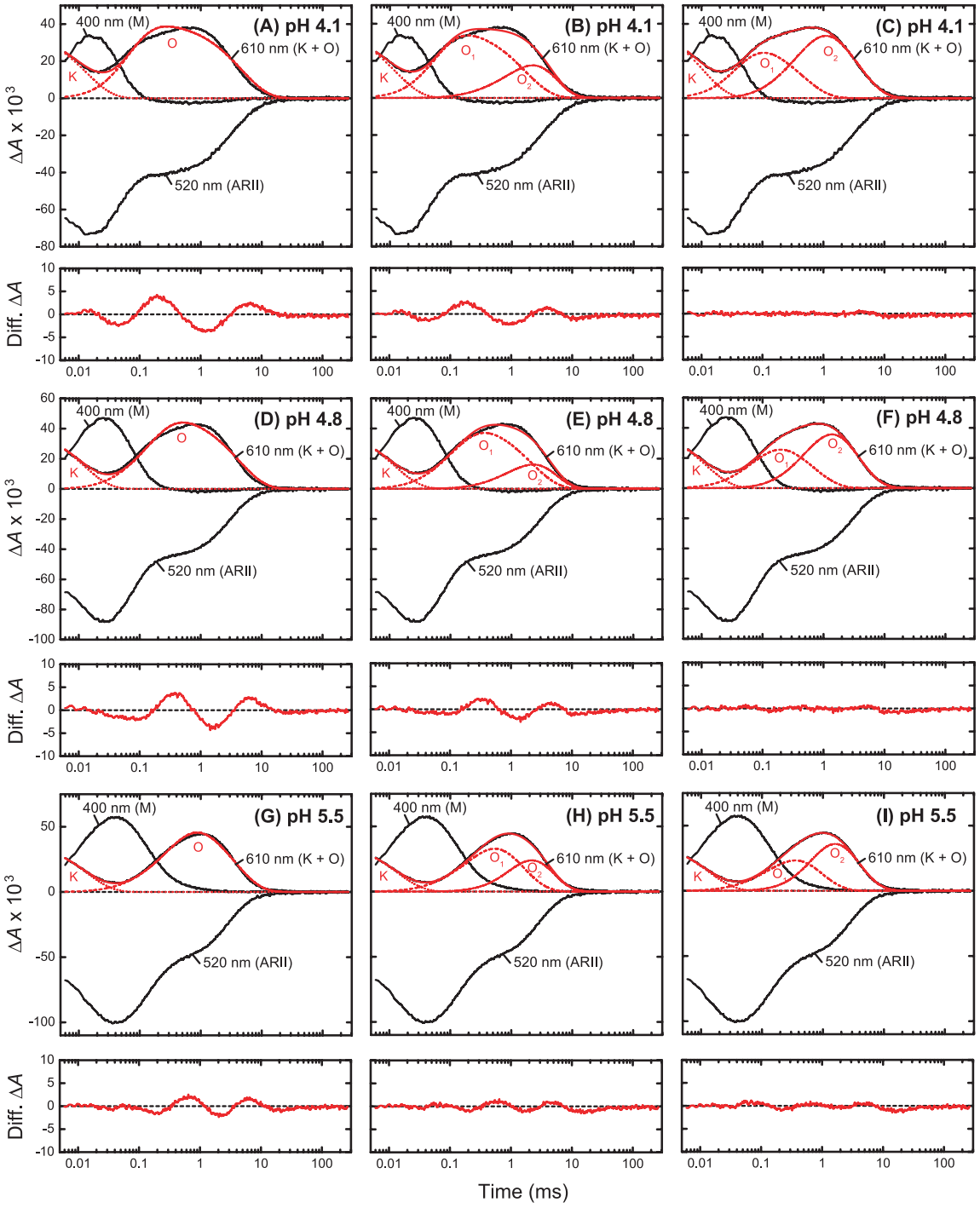

Figure 1 Simulation of the observed ΔA_{610} signal in the photocycle of ARII under acidic condition (pH≤5.5) by three analytical models. The data at pH 4.1 are analyzed by (A) a model with simple O (see Eq. (4)), (B) a model with two O-states, O_1 and O_2 ($\varepsilon_{O_1}=\varepsilon_{O_2}$) (see Eq. (6)), and (C) a model with O_1 and O_2 ($\varepsilon_{O_1}\neq\varepsilon_{O_2}$) (see Eq. (7)). The upper panels show the fitting results. In these figures, the observed and fitting curves are shown as black noisy and red smooth lines, respectively. The original state (ARII), M, and K plus O were monitored at 520, 400, and 610 nm, respectively. The red dotted, broken, and chain lines in these panels stand for the calculated fractional concentration changes of K, O_1 (or simple O), and O_2, respectively (see Eqs. (1), (3), and (5)). A small negative absorbance change in the ΔA_{400} signal at the time range from ~0.1 to ~10 ms may originate from the contribution of the small absorbance of the original pigment at this wavelength (also see Fig. 3B), which may lead to a fitting error with Eq. (2). The lower thin panels represent the difference at 610 nm between the observed and regression curves. The panels (D)–(F) and (G)–(I) show the corresponding fitting results for the data at pH 4.8 and 5.5, respectively. The assumptions are: a single O-intermediate (Eq. (4)) is adopted in the left column, two O-intermediates with the same ε (Eq. (6)) are in the middle column, and two O-intermediates with different εs (Eq. (7)) are in the right column. The ratio of α_{O_1} and α_{O_2} were estimated to be 0.63 and 0.64 at pH 4.8 and 5.5, respectively. Measurements were performed using the ARII protein solubilized by 0.05% DDM in medium containing 400 mM NaCl buffered with 2 mM 6-mixed buffer at 20°C.

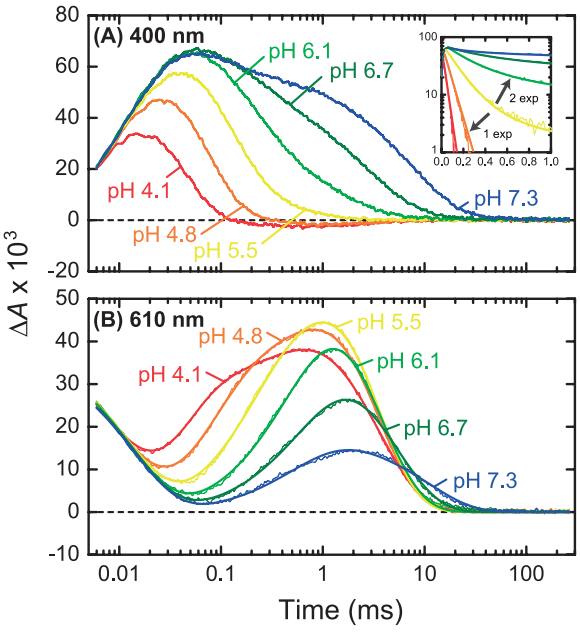

Figure 2 Coincidence of the pH-dependent appearance of M⇄N equilibrium and lack of detection of O_1-formation. Panels A and B show the pH-dependent changes of the ΔA_{400} and ΔA_{610} signals with an increase in pH from 4.1 to 7.3, respectively. The inset in panel A shows semilogarithmic plots of the ΔA_{400} signals. These data were obtained under the same experimental condition as described in Figure 1. The ΔA_{610} signals at pH≤5.5 are observed as a sum of K and two O substates (O_1, O_2), whereas those at pH>5.5 are approximated as a sum of K and simple O (O_2). The smooth curves show the fitting curves for the observed data (noisy lines) at each pH. The data regression at pH≤5.5 and above was done using Eq. (7) and (4). In near agreement with the pH-dependent change of the ΔA_{610} signal, the decay of the ΔA_{400} signal changes from mono- to bi-phasic, indicating the appearance of M⇄N equilibrium with increasing pH.

the decay of M (ΔA_{400}) is single exponential (see the data below pH 4.8 in the inset of Fig. 2A), and its decaying phase seems to match the rising phase of O (ΔA_{610}) (also see Table 1). When assuming that the concentration of K at the initial moment (t=0) is 1, the time-dependent fractional concentration changes of K, M, and O in the simplified scheme (K→M→O→) can be derived as the following equations, (1), (2) and (3), respectively.

$$\Delta K = e^{-k_0 t} \tag{1}$$

$$\Delta M = \frac{k_0}{k_1 - k_0}(e^{-k_0 t} - e^{-k_1 t}) \tag{2}$$

$$\Delta O = -\frac{k_0 k_1}{(k_0 - k_1)(k_1 - k_2)(k_2 - k_0)}[(k_1 - k_2)e^{-k_0 t} + (k_2 - k_0)e^{-k_1 t} + (k_0 - k_1)e^{-k_2 t}] \tag{3}$$

where k_0, k_1, and k_2 signify the rate constants of K-, M-, and O-decay, respectively. When scaling constants for the amplitude of the absorbance of K and O at 610 nm, which contain molar extinction coefficients (ε) for their respective intermediates, defined as α_K and α_O, respectively, ΔA_{610} signals can be expressed as the following equation.

$$\Delta A_{610} \approx \alpha_K \Delta K + \alpha_O \Delta O \tag{4}$$

Eq. (4) was applied to the analysis for the ΔA_{610} signal. This analysis, however, did not give a good fitting result (see Fig. 1A, D, and G). As seen in the lower panels of these figures, the fitting deviation is especially prominent in the absorbance change originating from the rise and decay of O (the time region from ~0.02 to ~10 ms). At first glance, the rise of O is not monophasic, irrespective of the single decay of M (see the strain line in the inset of Fig. 2A). This discrepancy can be solved by assuming a scheme that contains another O-like state after the first O, and these two sequential O-states are referred to as O_1 and O_2.

In the alternative scheme designed above (K→M→O_1→O_2→), the rise and decay rate constants of the two O substates were redefined as k_1 for O_1-rise, k_2 for O_1-decay (O_2-rise), and k_3 for O_2-decay. The time-dependent fractional concentration change of O_1 can be represented by Eq. (3), whereas that of O_2 can be derived as the following equation.

$$\Delta O_2 = -\frac{k_0 k_1 k_2}{(k_0 - k_1)(k_1 - k_2)(k_2 - k_0)(k_3 - k_0)(k_3 - k_1)(k_3 - k_2)} \begin{bmatrix} (k_1 - k_2)(k_3 - k_1)(k_3 - k_2)e^{-k_0 t} \\ +(k_2 - k_0)(k_3 - k_0)(k_3 - k_2)e^{-k_1 t} \\ +(k_0 - k_1)(k_3 - k_0)(k_3 - k_1)e^{-k_2 t} \\ +(k_0 - k_1)(k_1 - k_2)(k_2 - k_0)e^{-k_3 t} \end{bmatrix} \tag{5}$$

Table 1 Decay rate constants of various photointermediates under acidic conditions[a]

	k_0 (K-decay)	$k_{0'}$[b] (K-decay)	$k_{1'}$[b] (M-decay)	k_1 (M-decay)	k_2 (O_1-decay)	k_3 (O_2-decay)
pH 4.1	99.3	79.8	40.0	30.2	2.25	0.285
pH 4.8	86.4	66.8	17.7	13.1	1.53	0.324
pH 5.5	74.8	67.7	6.08	5.46	1.36	0.340

[a] The unit of all values is ms^{-1}.
[b] $k_{0'}$ and $k_{1'}$ were estimated by the fitting for the ΔA_{400} signals with Eq. (2) and distinguished from the corresponding values (k_0 and k_1) estimated from the fitting for the ΔA_{610} signals. Two k_0 and k_1 values are similar each other, although there are small differences between them presumably due to fitting error for the ΔA_{400} signals (also see the legend of Fig. 1).

We first performed fitting analysis using the following equation under the assumption that the εs for the two O-states are equal.

$$\Delta A_{610} \approx \alpha_K \Delta K + \alpha_O(\Delta O_1 + \Delta O_2) \quad (6)$$

This fitting result is shown in Figure 1B, E, and H. The fit is largely improved, but a small difference is yet observed (see the lower thin panels of Fig. 1B, E, and H).

Careful inspection reveals a small second increasing phase in the ΔA_{610} signal originating from O, which may imply that the ε of the second O (O_2) is different from that of the first one (O_1). Moreover, the results of the multiexponential global fitting analysis under acidic conditions (pH 5.0) also support this idea (see Fig. 3). This analysis reveals a photocycle scheme containing five photointermediates: P_0 (ARII)$\rightarrow P_1$ (K)$\rightarrow P_2$ (M)$\rightarrow P_3$ (O_1)$\rightarrow P_4$ (O_2)$\rightarrow P_5$ (ARII′) $\rightarrow P_0$ (ARII), which is almost consistent with the above described scheme, although a small contamination of K is observed in the P_2-state. The maximum absorbance of P_4 (O_2) is apparently larger than that of P_3 (O_1). Therefore, this together with the discrepancy of Eq. (6) with observed data led us to consider that ε_{O_i} (*i.e.* α_{O_i}) are different each other. The following combined function of Eqs. (1), (3), and (5) was used for the fitting.

$$\Delta A_{610} \approx \alpha_K \Delta K + \alpha_{O_1} \Delta O_1 + \alpha_{O_2} \Delta O_2 \quad (7)$$

Eq. (7) simulates the observed ΔA_{610} signal well (see Fig. 1C, F, and I). Therefore, we concluded that there were two O-intermediates with different α values. The estimated values of the k_is (i=0–3) are shown in Table 1. The values of α_{O_1} and α_{O_2} at pH 4.1 were 30.3 and 45.3, respectively, and the ratio of these values ($\alpha_{O_1}/\alpha_{O_2}$) was 0.67. This approximately 0.7 value is reflected by the ratio of ε_{O_1} to ε_{O_2}, which is almost the same as the ratio of the peak values (Fig. 3B and C).

As the medium pH increases, the rise of O becomes monophasic (see the lower panel B in Fig. 2). This may be attributed to the lack of accumulation of O_1 due to the prolonged decay of its precursor (N). Indeed, it appears that lack of contribution of O_1-formation to the ΔA_{610} signal occurs simultaneously with the appearance of the biphasic M-decay in the ΔA_{400} signal originating from the formation of M-N equilibrium due to the delay of N-decay, which was detectable at a pH above ~5.5 (Fig. 2). Thus, ΔA_{610} signals are observed as a sum of K and simple O (O_2) at a physiological neutral or weak alkaline pH. However, we infer that O_1 exists even under these pH conditions, although it cannot be detected because of the appearance of the M-N-O quasi-equilibrium. It is worth noting that Chizhov *et al.* reported the existence of two Os in HR from *Natronomonas pharaonis* (NpHR) [13].

What molecular event does occur during the transition from O_1 to O_2? Wang *et al.* proposed the following two possible sequences at the N→O transition of BR [9]:

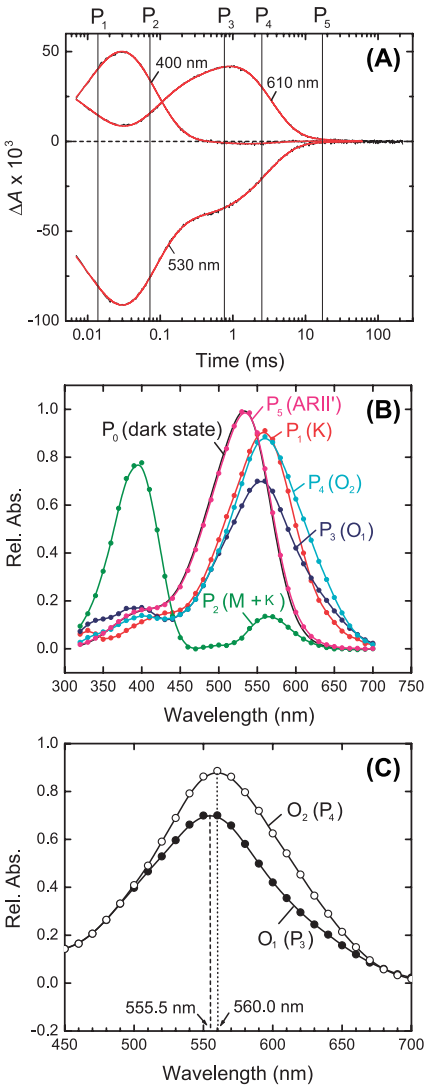

Figure 3 Global fitting analysis for the flash photolysis data in ARII at pH 5.0. (A) Flash-induced absorbance changes at three chosen wavelengths (400, 530, and 610 nm). The data were obtained in a solution containing 0.05% DDM, 400 mM NaCl and 10 mM 6-mixed buffer at 20°C. The observed data and multiexponential fitting curves are shown as black and red lines, respectively. These two curves are nearly completely overlapping. The vertical lines stand for the decay time constants of five kinetically defined states (P_1–P_5). (B) Relative absorbance spectra of P_0–P_5. Data analysis was performed for the obtained dataset at 320–700 nm with a 10 nm interval according to a sequential irreversible model including five P-states ($P_0\rightarrow P_1\rightarrow \ldots \rightarrow P_5\rightarrow P_0$, where P_0 denotes the dark state). The detailed procedures of this analysis should be referred to our previous papers [12,24,25]. (C) Closeup view of O_1- and O_2-spectra around the absorption peak. As seen in the panel B, P_3 and P_4 are composed of only red-shifted absorbance band (λ_{max} ~560 nm), suggesting that these states can be identified as O. With the P_3 to P_4 conversion, the λ_{max} of the spectrum almost does not change (Exactly, as shown in the panel C, that of P_3 is shorter by small difference (~5 nm) than that of P_4), but its maximum value increases from approx. 0.7 to 0.9 despite the lack of contribution from other absorption bands. Therefore, this may imply that the ε of O in P_3 (O_1) is different from that in P_4 (O_2). The ratio of their amplitudes at λ_{max} ($\varepsilon_{3,max}/\varepsilon_{4,max}$) is 0.78. The reason for the discrepancy between this value and that described in the text (*ca.* 0.7) is unclear, but may be experimental due to error.

1) Sequence 1: N (13-*cis* RET, 15-*anti* SBH^+)
→ (all-*trans* RET, 15-*syn* SBH^+)
→ (all-*trans* RET, 15-*anti* SBH^+),

2) Sequence 2: N (13-*cis* RET, 15-*anti* SBH^+)
→ (13-*cis* RET, 15-*syn* SBH^+)
→ (all-*trans* RET, 15-*anti* SBH^+).

The MD simulation by Wang *et al*. showed the possibility of Sequence 2 and the interaction of N-H with deprotonated $D212^{BR}$ was pointed out [9]. Furthemore, all-*trans* RET, 15-*syn* SBH^+ in Sequence 1 is considered to be metastable [14]. Considering these facts, Sequence 2 may be more plausible. As a broadly received conception, the O-state in BR has a twisted all-*trans* RET [15] and the large spectral red-shift during the N-O transition is attributed to the isomerization of RET from 13-*cis* to all-*trans*. In contrast, Subramaniam and coworkers reported the long life-time of O with 13-*cis* RET in $L93A^{BR}$ mutant which induces the slow reisomerization of RET due to abolishment of van der Waals interaction between the 13-methyl of RET and the terminal methyl groups of $L93^{BR}$ [16]. In addition, Zhang *et al.* solved its X-ray crystal structure and concluded that this long-lived O took 13-*cis* RET, 15-*syn* SBH^+ configuration [17]. These findings demonstrate at least the existence of a 13-*cis* O in $L93A^{BR}$. Tóth-Boconádi *et al.* presumed two substates of O in $L93A^{BR}$, and described that their distinction is the difference of the configuration of RET, 13-*cis* or all-*trans* [18,19]. Furthermore, Milder postulated the presence of two consecutive O-intermediates having 13-*cis* and all-*trans* RET in the wild-type BR [20]. Hence, the O_1-to-O_2 transition in this study may be also accompanied by the *cis*-to-*trans* isomerization of RET. In this respect, we can see that in Figure 3B, λ_{max} of P_3 (O_1) is a little bit smaller than P_4 (O_2) (also see Fig. 3C), and that ε of P_3 (O_1) is clearly smaller than the other. The 13-*cis* isomer in the dark-adapted BR has smaller λ_{max} and ε values compared with those of the all-*trans* isomer [21]. Other microbial rhodopsins such as HR from *Halobacterium salinarum* and *Anabaena* sensory rhodopsin showed similar characteristic [22,23]. This spectral property is consistent with the assumption that O_1 and O_2 take the RET configuration of 13-*cis* and all-*trans*, respectively. In the anion-pumping photocycle of NpHR proposed by Kouyama *et al.*, two O-intermediates (O′ and O) with 13-*cis* and -*trans* form of RET were assumed [5], which is also consistent with our present assumption. Thus, together with the model by Wang *et al.* [9], we propose a conformational scheme of RET and SBH^+ upon the transition from N to O, which is shown in Figure 4.

In the acidic condition adopted here, N-decay is very fast and the rate of the isomerization is relatively pH-independent, which may result in the observation of O_1. Under neutral or alkaline conditions, N-decay is slow and the O_1-to-O_2 conversion rate is presumably faster, which results in the lack of detection of O_1. Allthough O-intermediate in the crystal

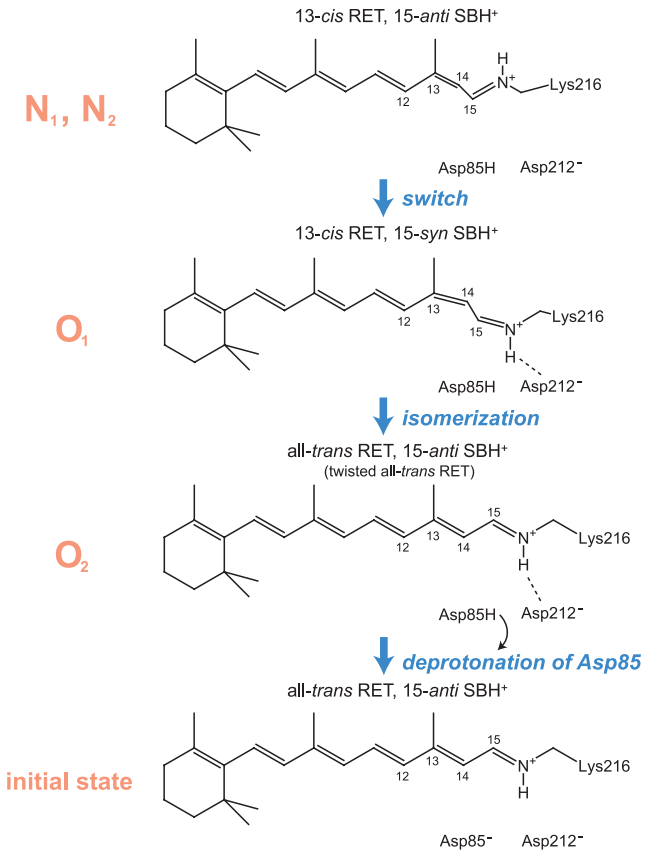

Figure 4 Schematic of configuration change of RET and SBH^+ in the latter half of the photocycle. A picture is depicted in the case of BR.

structure of $L93A^{BR}$ takes 13-*cis* RET, 15-*syn* SBH^+ in agreement with the expected configuration of O_1 in the present paper [17], the precise RET configuration of O_1 of the wild-type BR should be determined in further study. In addition, we should explore its existence for other microbial rhodopsins. However, there is a possibility that in many microbial rhodopsins, observation of O_1 (13-*cis* RET, 15-*syn* SBH^+) is difficult (although its existence is in the case) maybe due to M-N-O equilibrium and/or its short life time. In this case, a problem arises why this intermediate can be observable in ARII. This is an intriguing subject in future.

Conclusion

In this study, we analyzed the photocycle of ARII under acidic conditions (pH ≤ 5.5) at which accumulation of N is almost negligible. The kinetic analysis with three models revealed that the scheme containing two sequential O-intermediates (O_1 and O_2) with different ε values is best. Considering the smaller λ_{max} and ε of O_1 than those of O_2, we expected that the O_1-to-O_2 transition is accompanied by the RET isomerization from 13-*cis* to all-*trans*, which agrees with the proposed sequence of two configurational changes in RET and SBH^+ based on the MD simulations by Wang

et al. [9]: thermal reisomerization of RET is preceded by switch of the accessibility of SBH^+. Whether there are two O-intermediates in the photocycle of other microbial rhodopsins including BR should be investigated in future. However, the presence of the M-N-O equilibrium may make the detection of the first O (O_1 in the present study) difficult.

Acknowledgement

This work was supported by the Targeted Proteins Research Program and grants from the Japanese Ministry of Education, Culture, Sports, Science, and Technology to K. S. (19770136) and N. K. (22590049).

Conflicts of Interest

All authors declare that they have no conflict of interest.

Author Contributions

J. T., T. K., K. S., and N. K. directed the research. J. T. and N. K. co-wrote the manuscript. K. S. prepared ARII samples. T. K. performed flash photolysis measurements. J. T. and T. K. analyzed flash photolysis data. T. N., M. D., T. K.-S., M. S., S. Y., and S. M. helped to draft the manuscript. All author critically reviewed and approved the final manuscript.

References

[1] Ernst, O. P., Lodowski, D. T., Elstner, M., Hegemann, P., Brown, L. S. & Kandori, H. Microbial and animal rhodopsins: structures, functions, and molecular mechanisms. *Chem. Rev.* **114**, 126–163 (2014).

[2] Chizhov, I., Chernavskii, D. S., Engelhard, M., Mueller, K.-H., Zubov, B. V. & Hess, B. Spectrally silent transitions in the bacteriorhodopsin photocycle. *Biophys. J.* **71**, 2329–2345 (1996).

[3] Lanyi, J. K. Bacteriorhodopsin. *Annu. Rev. Physiol.* **66**, 665–688 (2004).

[4] Shibasaki, K., Shigemura, H., Kikukawa, T., Kamiya, M., Aizawa, T., Kawano, K., *et al.* Role of Thr218 in the light-driven anion pump halorhodopsin from *Natronomonas pharaonis*. *Biochemistry* **52**, 9257–9268 (2013).

[5] Kouyama, T., Kawaguchi, H., Nakanishi, T., Kubo, H. & Murakami, M. Crystal structures of the L_1, L_2, N, and O states of *pharaonis* halorhodopsin. *Biophys. J.* **108**, 2680–2690 (2015).

[6] Klare, J. P., Gordeliy, V. I., Labahn, J., Büldt, G., Steinhoff, H.-J. & Engelhard, M. The archaeal sensory rhodopsin II/transducer complex: a model for transmembrane signal transfer. *FEBS Lett.* **564**, 219–224 (2004).

[7] Inoue, K., Sudo, Y., Homma, M. & Kandori, H. Spectrally silent intermediates during the photochemical reactions of *Salinibacter* sensory rhodopsin I. *J. Phys. Chem. B* **115**, 4500–4508 (2011).

[8] Haupts, U., Tittor, J., Bamberg, E. & Oesterhelt, D. General concept for ion translocation by halobacterial retinal proteins: the isomerization/switch/transfer (IST) model. *Biochemistry* **36**, 2–7 (1997).

[9] Wang, T., Facciotti, M. T. & Duan, Y. Schiff base switch II precedes the retinal thermal isomerization in the photocycle of bacteriorhodopsin. *PLoS ONE* **8**, e69882 (2013).

[10] Wada, T., Shimono, K., Kikukawa, T., Hato, M., Shinya, N., Kim, S. Y., *et al.* Crystal structure of the eukaryotic light-driven proton-pumping rhodopsin, *Acetabularia* rhodopsin II, from marine alga. *J. Mol. Biol.* **411**, 986–998 (2011).

[11] Kikukawa, T., Shimono, K., Tamogami, J., Miyauchi, S., Kim, S. Y., Kimura-Someya, T., *et al.* Photochemistry of *Acetabularia* rhodopsin II from a marine plant, *Acetabularia acetabulum*. *Biochemistry* **50**, 8888–8898 (2011).

[12] Sato, M., Kubo, M., Aizawa, T., Kamo, N., Kikukawa, T., Nitta, K., *et al.* Role of putative anion-binding sites in cytoplasmic and extracellular channels of *Natronomonas pharaonis* halorhodopsin. *Biochemistry* **44**, 4775–4784 (2005).

[13] Chizhov, I. & Engelhard, M. Temperature and halide dependence of the photocycle of halorhodopsin from *Natronobacterium pharaonis*. *Biophys. J.* **81**, 1600–1612 (2001).

[14] Brown, L. S., Dioumaev, A. K., Needleman, R. & Lanyi, J. K. Local-access model for proton transfer in bacteriorhodopsin. *Biochemistry* **37**, 3982–3993 (1998).

[15] Smith, S. O., Pardoen, J. A., Mulder, P. P. J., Curry, B., Lugtenburg, J. & Mathies, R. Chromophore structure in bacteriorhodopsin's O_{640} photointermediate. *Biochemistry* **22**, 6141–6148 (1983).

[16] Delaney, J. K., Schweiger, U. & Subramaniam, S. Molecular mechanism of protein-retinal coupling in bacteriorhodopsin. *Proc. Natl. Acad. Sci. USA* **92**, 11120-11124 (1995).

[17] Zhang, J., Yamazaki, Y., Hikake, M., Murakami, M., Ihara, K. & Kouyama, T. Crystal structure of the O intermediate of the Leu93→Ala mutant of bacteriorhodopsin. *Proteins* **80**, 2384–2396 (2012).

[18] Tóth-Boconádi, R., Keszthelyi, L. & Stoeckenius, W. Late events in the photocycle of bacteriorhodopsin mutant L93A. *Biophys. J.* **84**, 3848–3856 (2003).

[19] Tóth-Boconádi, R., Keszthelyi, L. & Stoeckenius, W. Photoexcitation of the O-intermediate in bacteriorhodopsin mutant L93A. *Biophys. J.* **84**, 3857–3863 (2003).

[20] Milder, S. J. Correlation between absorption maxima and thermal isomerization rates in bacteriorhodopsin. *Biophys. J.* **60**, 440–446 (1991).

[21] Oesterhelt, D., Meentzen, M. & Schuhmann, L. Reversible dissociation of the purple complex in bacteriorhodopsin and identification of 13-*cis* and all-*trans*-retinal as its chromophores. *Eur. J. Biochem.* **40**, 453–463 (1973).

[22] Yamashita, Y., Kikukawa, T., Tsukamoto, T., Kamiya, M., Aizawa, T., Kawano, K., *et al.* Expression of *salinarum* halorhodopsin in *Escherichia coli* cells: Solubilization in the presence of retinal yields the natural state. *Biochim. Biophys. Acta* **1808**, 2905–2912 (2011).

[23] Rozin, R., Wand, A., Jung, K.-H., Ruhman, S. & Sheves, M. pH dependence of Anabaena sensory rhodopsin: retinal isomer composition, rate of dark adaptation, and photochemistry. *J. Phys. Chem. B* **118**, 8995–9006 (2014).

[24] Hasegawa, C., Kikukawa, T., Miyauchi, S., Seki, A., Sudo, Y., Kubo, M., *et al.* Interaction of the halobacterial transducer to a halorhodopsin mutant engineered so as to bind the transducer: Cl^- circulation within the extracellular channel. *Photochem. Photobiol.* **83**, 293–302 (2007).

[25] Tateishi, Y., Abe, T., Tamogami, J., Nakao, Y., Kikukawa, T., Kamo, N, *et al.* Spectroscopic evidence for the formation of an N intermediate during the photocycle of sensory rhodopsin II (phoborhodopsin) from *Natronobacterium pharaonis*. *Biochemistry* **50**, 2135–2143 (2011).